MR Based Limited-field-of-view SPECT Image Reconstruction

K. S. Lee[1,2], W. W. Roeck[1,3], G. T. Gullberg[4], and O. Nalcioglu[1,3]

[1]Tu & Yuen Center for Functional Onco-Imaging, University of California, Irvine, Irvine, CA, United States, [2]Department of Electrical Engineering and Computer Science, University of California, Irvine, Irvine, CA, United States, [3]Department of Radiological Sciences, University of California, Irvine, Irvine, CA, United States, [4]Ernest Orlando Lawrence Berkeley National Laboratory, Berkeley, CA, United States

Introduction

The rationale for multi-modality imaging is to integrate the strengths of different imaging technologies while reducing the shortcomings of an individual modality [1]. In nuclear imaging the target area is usually smaller than the entire object thus focusing the detector on the LFOV results in various advantages including the use of a smaller nuclear detector (less cost), smaller reconstruction region (faster reconstruction), and higher spatial resolution when used in conjunction with pinhole collimators with magnification. The work presented here proposes a limited-field-of-view (LFOV) SPECT image reconstruction technique, hereafter called the Keyhole SPECT (K-SPECT) method that can be implemented on images obtained from a simultaneous multi-modality MR/SPECT system for small animal imaging. K-SPECT uses *a priori* information from the full field-of-view (FOV) MRI and original SPECT image reconstructed without any *a priori* information.

Methods

1.Simultaneous MR and SPECT image acquisition and identification of the region of interest in K-SPECT from the high resolution MR image: The proposed LFOV MR/SPECT system consists of a 4T MR research system and an LFOV pinhole SPECT system with all the MR-compatible components, including a 9-pinhole collimator, and proper RF shielding. The SPECT goes inside the MR system as shown in Fig.1. MR and SPECT images are acquired simultaneously. The region of interest (ROI) that covers the target organ needs to be determined from the MR images. This is done by performing a whole body MRI and then selecting a 3D spherical volume of interest (VOI) from these images to cover the target region (left in Fig.1). Once the VOI is determined from the MR images, the animal bed can be moved to position the VOI at the center of the LFOV of the SPECT system (right in Fig.1).

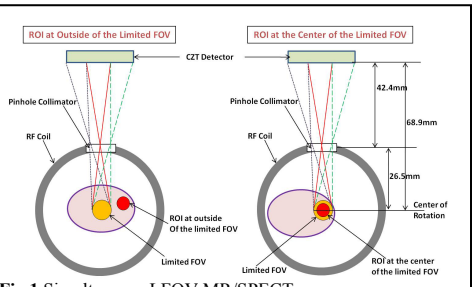

Fig.1 Simultaneous LFOV MR/SPECT

2. ML-EM SPECT image reconstruction without using a priori: At first the system matrix was generated for the 9-pinhole SPECT system using 64x64x128 pixels and 90 equally spaced axial angular views over 360-degrees. We used the Maximum Likelihood - Expectation Maximization (ML-EM) technique [2] for image reconstruction.

$$\lambda_j^{n+1} = \frac{\lambda_j^n}{\sum_m S_{m,j}} \sum_i S_{i,j} \frac{Q_i}{\sum_k S_{i,k} \lambda_k^n} \qquad \text{Eq. (1)}$$

where Q_i is the measured value for the projection bin i, λ_j^n is the reconstructed value in voxel j at the n^{th} iteration, $S_{i,j}$ is the sensitivity matrix for the contribution of voxel j to projection bin i .

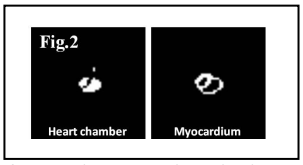

3. Determination of the adaptive weighting matrix using a priori information from the initial SPECT image: Although the signal intensity distribution in MRI is different from the SPECT image due to the different physical and biological origins for each signal, MRI can still provide a high-resolution anatomical image of the target region. Once the ROI is determined from the MR image, it can be used to form a template to separate the target and non-target regions in the SPECT image reconstruction. The segmented ROIs from MR images are shown in Fig.2 as examples.

$$S'_{i,j} = \sum_k S_{i,k} \xi_{k,j} \qquad \text{Eq. (2)}$$

where

$$\xi_{k,j} = \begin{cases} T/B & if \quad (k,j) \in \text{target} \\ 1 & if \quad (k,j) \in \text{LFOV} \cap \text{target}^c \\ 0 & if \quad (k,j) \in \text{LFOV}^c \end{cases} \qquad \text{Eq. (3)}$$

$$\lambda_j^{n+1} = \frac{\lambda_j^n}{\sum_m S'_{m,j}} \sum_i S'_{i,j} \frac{Q_i}{\sum_k S'_{i,k} \lambda_k^n} \qquad \text{Eq. (4)}$$

4. Generation of adaptive system matrix by using two priors: The average counts in the target and background regions are calculated from the initial SPECT image, and then assigned to a weighting matrix, $\xi_{k,j}$, to generate adaptive system matrix as shown in Eqs. (2) and (3).

5. *Image reconstruction using adaptive system matrix using ML-EM:* The SPECT image reconstruction using ML-EM is performed with using the modified system matrix, $S'_{i,j}$, for the LFOV as shown in Eq. (4).

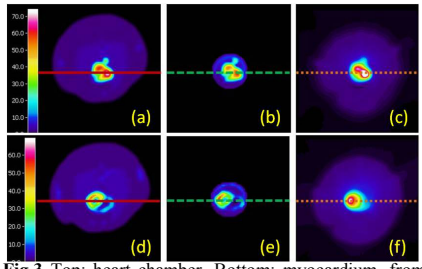

Fig.3 Top: heart chamber, Bottom: myocardium. from left, phantom, reconstructed images using K-SPECT method. and using standard ML-EM.

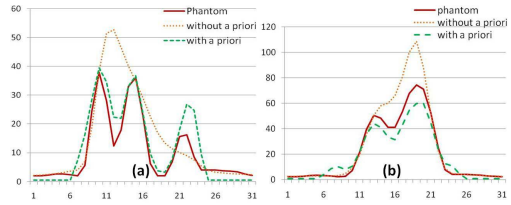

Fig.4 Line profiles for (a) heart chamber, and (b) myocardium in Fig.3. Color and shape of each line corresponds to the lines passing through images in Fig.3. The graphs show that the two chambers are separable in images with K-SPECT, but not in images with standard ML-EM.

Simulation and Results

Simulation with the digital mouse whole body (MOBY) phantom: The image reconstructions were performed with the 3-D MOBY phantoms that were generated with high radioactivity in the heart chamber (Fig.3 (a)) and myocardium (Fig.3 (d)). Images shown in Fig.3 are the center slice of 3-D volume images. The images in Fig.3 (b)-(c) and (e)-(f) and graphs in Fig.4 show that K-SPECT improves the image resolution and quality.

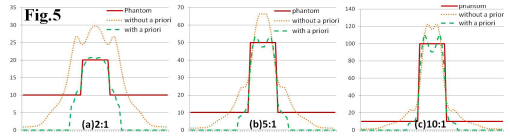

Simulation with various target-to-background ratios: The digital phantoms with various target-to-background (T/B) ratios were generated and reconstructed using K-SPECT method. The results are shown in Figs. 5 and 6. The graphs and images show that higher the T/B ratio results the better K-SPECT reduces artifacts caused by activities outside the LFOV.

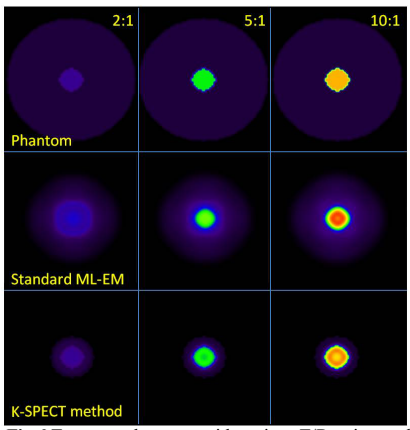

Fig.6 Top row: phantoms with various T/B ratios, and reconstructed images with; middle row: standard ML-EM, bottom row: K-SPECT

Discussion and Conclusion

In these simulations, the SPECT image reconstructions were performed with using the boundary information of the ROI that was determined by high-resolution MR images. The simulation results with digital mouse phantoms show that the K-SPECT method improved image quality and accuracy in the SPECT images by 48.5% for heart chamber and 52.6% for myocardium. The simulations with various T/B ratios indicate that the normalized root-mean-square-error by target activity are 0.34%, 0.25%, and 0.15% for T/B ratios of 2:1, 5:1, and 10:1, respectively. As shown in Fig. 5, K-SPECT works better on images with high T/B ratios, which are common in nuclear imaging. Unlike other studies that are using anatomical images for attenuation correction or post image processing, the Keyhole SPECT method uses *a priori* information from MRI at the image reconstruction level.

References: [1] Cherry, S.R. Ann. Rev. Biomed. Eng. **8** 35-62 (2006) [2] Shepp, L. A., and Vardi, Y. *IEEE Trans. Med. Imag.*, Vol. **1**(2), pp. 113-122(1982)